Delft University of Technology

Monolithic binary stiffness building blocks for mechanical digital machines

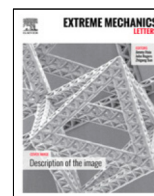Kuppens, P. R.; Bessa, M. A.; Herder, J. L.; Hopkins, J. B.

Important note
To cite this publication, please use the final published version (if applicable).
Please check the document version above.

Monolithic binary stiffness building blocks for mechanical digital machines

P.R. Kuppens [a],[*], M.A. Bessa [a],[1], J.L. Herder [a],[2], J.B. Hopkins [b],[3]

[a] *Delft University of Technology, Mekelweg 2, Delft, The Netherlands*
[b] *University of California, Los Angeles, 420 Westwood Plaza Eng. IV 46-147F Los Angeles, CA 90095, USA*

ARTICLE INFO

ABSTRACT

We introduce two essential building blocks with binary stiffness for mechanical digital machines. The large scale fully compliant mechanisms have rectilinear and rotational kinematics and use a new V-shaped negative stiffness structure to create two extreme states of stiffness by static balancing. The use of a mechanical bistable switch allows us to toggle between near-zero-stiffness and high-stiffness states, effectively turning off and on stiffness. A stiffness reduction of 98.8% and 99.9% is achieved for linear and rotary motion over a range of 13.3% (20 mm) and 0.4 rad (23°) respectively. Stiffness states can be reversibly changed by toggling the mechanical switch, or irreversibly by actuating the main stage.

These binary stiffness mechanisms could set the stage for a new type of mechanical logic, adaptive and programmable metamaterials and other types of digital mechanical devices. Practical mechanical digital machines and materials require miniaturized and easily micro-manufactured components. We have therefore carefully considered scalability by integrating all required structures into a planar and monolithic architecture. This allows miniaturization and fabrication with conventional surface-micromachining and additive manufacturing such as photolithography, two-photon lithography and fused deposition modeling.

1. Introduction

Mechanisms with variable stiffness have the ability to change their stiffness over a range of values. This can be done actively and passively in a multitude of different ways. For example, electrostatically, piezoelectrically, thermally and mechanically [1]. They are commonly used in microelectromechanical system (MEMS) [1], vibration isolation [2] and variable impedance actuators [3] for example for human friendly robots [4] and robot fingers [5].

More recently variable stiffness is used to create metamaterials where controlled changes in local stiffness enable adaptive bulk properties. Examples are architectured materials with multiple Poisson's ratios [6], variable stiffness [7,8] as well as robotic materials with programmable properties [9–11]. These materials exploit variable stiffness created by geometry [6], phase change [7], fluid channels [8] or by active feedback control of thermal actuators [9–11].

Instead of continuously variable stiffness mechanisms, binary stiffness mechanisms may be used. A binary stiffness mechanism can only change its stiffness between two different values that ideally have an infinite ratio. Two extremely different states of stiffness can be created by static balancing [12,13]. It uses negative stiffness caused by preloading to counteract a positive stiffness elsewhere in the mechanism. Even though the upper limit of the stiffness is limited by bulk properties, the ratio between the upper and lower limit can be infinite if the lower limit is reduced to zero stiffness [14]. Zero stiffness can be achieved if negative stiffness is designed to be equal but opposite to the positive stiffness. Different techniques may be used such as preloading in postbuckling [15] or up to the critical buckling load [16], zero-free-length springs [17,18] and curved surfaces [19,20], see [21, 22] for an extensive overview. Binary states of stiffness can thus be achieved by enabling and disabling static balancing by engaging and disengaging preloading, effectively turning the stiffness off and on.

Programmable zero stiffness based on multistable mechanisms [23–25] has been previously reported in [26]. However, the reported device is not of a digital nature, since the flexible programming inputs are analog and require a sustained holding

---

* Correspondence to: Dept. Precision and Microsystems Engineering, The Netherlands.

E-mail address: p.r.kuppens@tudelft.nl (P.R. Kuppens).

[1] Dept. Materials Science and Engineering.
[2] Dept. Precision and Microsystems Engineering.
[3] Dept. Mechanical and Aerospace Engineering

force to create both low or high stiffness. In addition, the zero stiffness (and zero force) monostable behavior is obtained in prebuckling which limits the low stiffness to small deflections, i.e. the zero-stiffness is instantaneous.

If binary stiffness mechanisms are used in large numbers, they may approach continuous properties and enable new types of digital mechanical machines and metamaterials [27]. Examples could include novel computing systems based on mechanical logic that could potentially be build on the molecular level [28, 29] and provide more robustness in extremely harsh environments such as high radiation, because they lack a significant electromagnetic signature [30,28,31].

In most existing mechanical logic systems each Boolean state is associated with a predefined displacement of the mechanism, such as the location of a dial. Examples are rigid body logic [32], multi-stable micro-flexural additively manufactured logic gates [31] and micro-flexural NOT and AND gates [33,34]. All are examples of static logic, however in most modern computing systems dynamic logic is used because of its superior performance [35]. In dynamic logic a clocked signal is used to evaluate the state after input signals are applied, as opposed to static logic where the output is immediately available. An example of mechanical dynamic logic is rod logic [36]. It uses sliding rods that block or unblock each other to create logic states in terms of potential sliding motion evaluated by an oscillating mechanical signal [28]. We can regard the blocked and unblocked configurations as states of high and low stiffness such that one rod logical element is essentially a binary stiffness mechanism. A more recent example modulates the linear resonance frequency of an arch beam resonator electrothermally to perform various 2 bit and 3 bit logic operations [37].

Practical mechanical digital machines and materials require binary stiffness elements to be easily miniaturized and micro-manufactured, since large numbers are needed in a small volume. It is therefore essential to avoid any form of assembly and account for micro-manufacturing techniques like photolithography and upcoming 3D printing technologies such as two-photon lithography [38]. Necessary properties are therefore a fully mono-lithic and planar architecture which can be created by exploiting the flexibility of materials in what is known as a compliant mechanism.

In this paper we present two fully compliant binary stiffness mechanisms with large deflection linear and rotary motion based on static balancing. A new V-shaped negative stiffness structure is introduced that maximizes the ratio between high and low stiffness. The preloading required for negative stiffness is controlled by a reversible bistable switch independent of primary mobility. Kinematics are dictated by two parallel or angled plate springs.

The method for obtaining binary stiffness is first explained with compression springs and extended to a fully compliant mechanism by replacing them with buckled beams. Final mecha-nism dimensions are iteratively tuned by hand. This semi-autonomous process still relies on domain knowledge from the designer, but a fully automated process relying on machine learn-ing and optimization could be used, as demonstrated in a dif-ferent context [39]. Examples of design optimizations with this method include a supercompressible micro-structure [40] and an ultra-thin shell structure [41].

We have validated the designs by prototyping decimeter scale prototypes and performing mechanical tests. It is plausible that the presented designs can be scaled down to micro or nanoscale, because all required structures are planar and fully compliant and are integrated in a monolithic and planar device that avoids as-sembly. A scaled down version would rely on identical principles and only requires redesign for different material properties.

The mechanisms are stress free and in their high stiffness configuration when manufactured. Low stiffness is enabled when the bistable switch is engaged. This can be done irreversibly by actuating the main stage, or reversibly by toggling the bistable switch itself.

2. Method for binary stiffness

Binary variable stiffness is achieved by enabling and disabling static balancing. Static balancing is an approach to keep the potential energy in a system constant and consequently all net conservative forces and stiffness are zero [42]. It is achieved by adding an elastic structure with negative stiffness in parallel to the functional part with positive stiffness. If negative and positive stiffness exactly oppose, a net zero stiffness results. The required negative stiffness is a consequence of releasing elastic poten-tial energy previously inserted by preloading. Therefore, we can toggle between balanced zero stiffness and unbalanced positive stiffness by engaging and disengaging preloading.

In its simplest form, negative stiffness is created by axially preloading an ordinary compression spring from its initial length L_0 to L_p as shown in Fig. 1(a), note that $L_0 = h_0$ and $L_p = h_p$. This works for both linear [20,13] and rotational motion [43] of the cart. The potential energy of the spring as function of cart displacement u is given by:

$$E_I(u) = \frac{1}{2}k\left(\sqrt{\left(\mathbf{p}_c^T \cdot \mathbf{p}_c\right)} - L_0\right)^2 \tag{1}$$

where k is the spring stiffness, $\mathbf{p}_c = \left[u, h_p\right]^T$ the cart location, h_p the spring length at $u = 0$ and L_0 the initial length of the spring. Force and stiffness at the cart are given by:

$$F_I(u) = \frac{\mathrm{d}E_I(u)}{\mathrm{d}u}, \quad K_I(u) = \frac{\mathrm{d}^2 E_I(u)}{\mathrm{d}u^2} \tag{2}$$

E_I, F_I and K_I are shown in Fig. 1(e) with $k = 1$, without preloading ($h_0 = h_p = 2$) and with preloading ($h_0 = 2, h_p = 1$). It shows that for large values of u the stiffness K_I converges to k independent of preloading, i.e. $\lim_{u \to \infty} K_I\left(u, h_p\right) = k$. Also if the spring is stretched by large amounts ($h_p \gg L_0$) K_I converges to k independent of u, i.e. $\lim_{h_p \to \infty} K_I\left(u, h_p\right) = k$. However, since compliant mechanisms have limited stroke, we are interested in behavior around $u = 0$. And since negative stiffness is only created by compressing the spring, we are only interested in values of $0 \le h_p \le L_0$.

The stiffness K_I at $u = 0$ is given by:

$$K_I\left(u = 0\right) = -\frac{k\left(L_0 - h_p\right)}{h_p}, \quad h_p \ge 0 \tag{3}$$

which shows the stiffness $K_I\left(u = 0\right) = 0$ when $h_p = L_0$ and becomes more negative as h_p decreases , i.e.

$$\lim_{h_p \to 0} K_I(u = 0) = -\infty \tag{4}$$

This demonstrates the ability to turn negative stiffness on and off by controlling the preloading distance h_p. A compliant analog is obtained by axially preloading a continuum plate in post buck-ling [13] as shown in Fig. 1(b), possibly with various boundary conditions such as pinned–pinned [20], clamped–pinned [15,44] and clamped–clamped [44].

A preloaded continuum plate is in theory able to reduce the combined stiffness to zero, because the amount of negative stiff-ness can be tuned by changing its geometry [15]. In practice, perfectly matching positive and negative stiffness is hard and af-fected by modeling errors, manufacturing tolerances and nonlin-ear effects. It is therefore desirable to maximize the high stiffness state, because stiffness states become more distinguishable. This is done by increasing the stiffness without preloading around
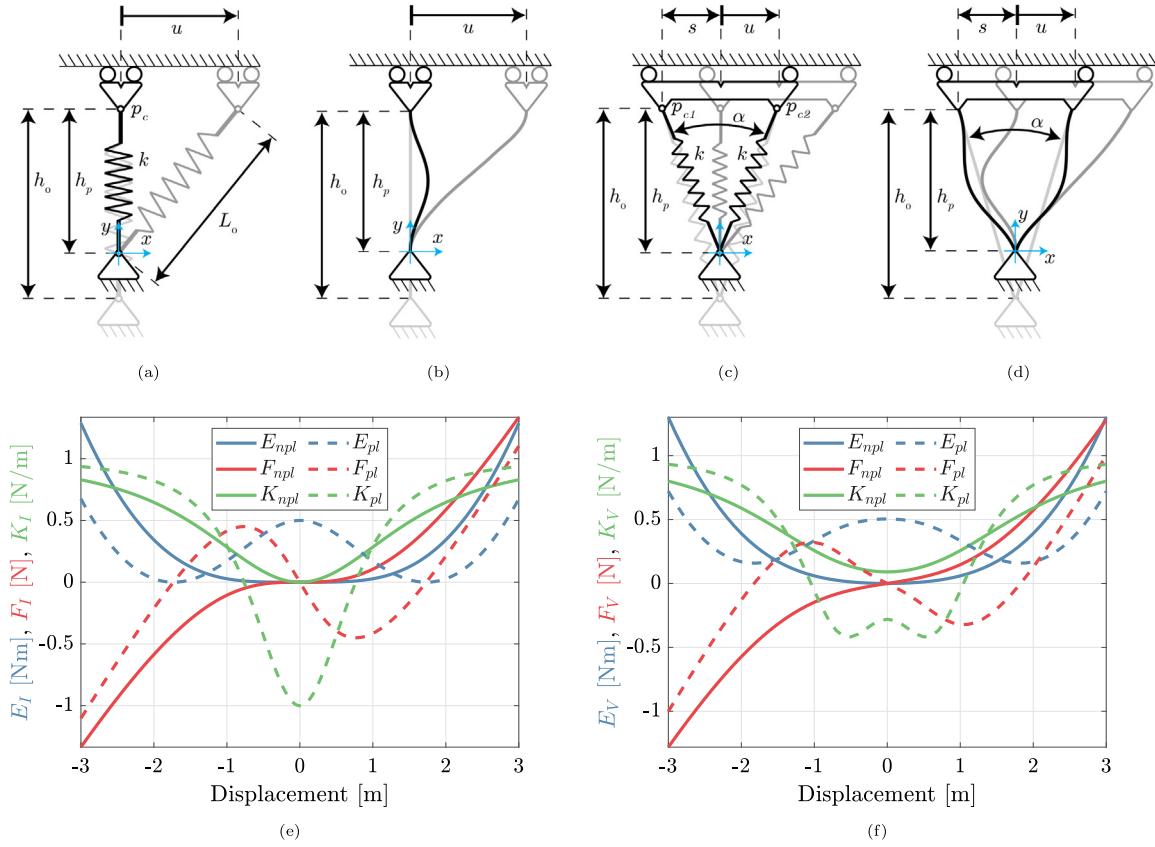
Fig. 1. (a) Shows a canonical example of a negative stiffness mechanisms and (b) its compliant equivalent. In (c) the single spring has been decomposed into two springs in a V-shaped orientation and (d) shows its compliant equivalent. (e) Shows the potential energy E_I, force F_I and stiffness K_I with and without preloading. (f) Shows the potential energy E_V, force F_V and stiffness K_V with and without preloading. Solid lines refer to cases without preloading while dashed lines with preloading. (For interpretation of the references to color in this figure legend, the reader is referred to the web version of this article.)

$u = 0$, while keeping the ability to generate negative stiffness when preloaded. Increasing the high stiffness state is done by decomposing the compression spring in a V-shaped configuration as shown in Fig. 1(c).

The potential energy of the V-shaped springs on a cart is given by:

$$E_V = \frac{1}{2}k\left(\sqrt{\mathbf{p}_{c1}^T\mathbf{p}_{c1}} - L_0\right)^2 + \frac{1}{2}k\left(\sqrt{\mathbf{p}_{c2}^T\mathbf{p}_{c2}} - L_0\right)^2 \quad (5)$$

where k is spring stiffness, the initial length $L_0 = \sqrt{h_0^2 + s^2}$, $\mathbf{p}_{c1} = [u - s, h_p]^T$, $\mathbf{p}_{c2} = [u + s, h_p]^T$, with $s \geq 0$ half the distance between the springs on the cart. Force F_V and stiffness K_V are computed by differentiation of E_V as in Eq. (2). They are shown in Fig. 1(f) with $k = 0.5, \alpha = 35°$, without preloading $h_p = h_0 = 2$ and with preloading $h_0 = 2$ and $h_p = s\sqrt{2}$.

The stiffness K_V at $u = 0$ is given by:

$$K_V(u = 0) = 2k\left(\frac{s^2}{L_p^2}\left(1 + \frac{L_0 - L_p}{L_p}\right) - \frac{L_0 - L_p}{L_p}\right) \quad (6)$$

where $L_p = \sqrt{h_p^2 + s^2}$. The minimum stiffness (i.e. max negative stiffness) achievable by preloading is determined by finding the roots of $\frac{dK_V(u=0)}{dh_p}$, which are given by $h_p = \pm s\sqrt{2}$. Substituting the positive value $h_p = s\sqrt{2}$ in Eq. (6) yields:

$$\min_{h_p} K_V(u = 0) = 2k - \frac{4kL_0}{3\sqrt{3}s}, \quad s \geq 0 \quad (7)$$

which shows that unbounded negative stiffness can be obtained for $\frac{2\sqrt{3}}{9}L_0 > s \geq 0$.

On the other hand, the stiffness without preloading ($L_0 = L_p$) is given by

$$K_V(u = 0) = 2k\frac{s^2}{L_p^2}, \quad s \geq 0 \quad (8)$$

which is positive for any nonzero s.

Eqs. (7) and (8) show that two springs placed in a V-shaped configuration can generate negative stiffness when preloaded yet have positive stiffness without preloading.

A compliant analog is shown in Fig. 1(d) which will be given exact dimension in an iterative design process. The advantage over a single or multiple vertical beams is the increased stiffness when not preloaded. Values for its negative and positive stiffness depend on geometry and preloading. Too much negative stiffness results in a combined system with negative stiffness. Too little negative stiffness and combined system stiffness is positive. Since we can continuously shift between these two behaviors, by changing for example V-shaped beam length or the geometry of the stage beams, an optimum can be found that results in zero combined stiffness.

2.1. Controlling the preloading

Preloading is easily controlled by hand in many macro-scale statically balanced mechanisms, for example during assembly [45] or by using linear stages [46,13]. On the micro-scale, preloading becomes a significant challenge because manual handling is difficult which makes assembly economically unjustifiable. Proposed monolithic solutions include shaking [47] and residual film stress [48], however these methods are irreversible. Reversible examples exist that make use of multistable compliant
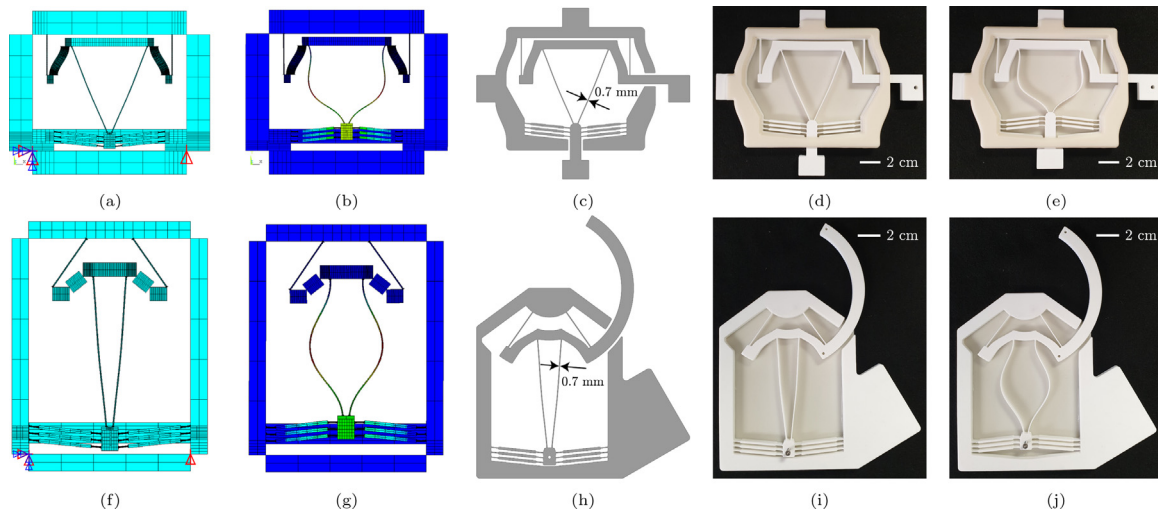
Fig. 2. (a, f) Element plots of the linear and rotary devices, (b, g) displacement solutions, (c, h) CAD drawings, (d, i) photos of the prototypes in the stiff state and (e, j) the prototype in the compliant state.
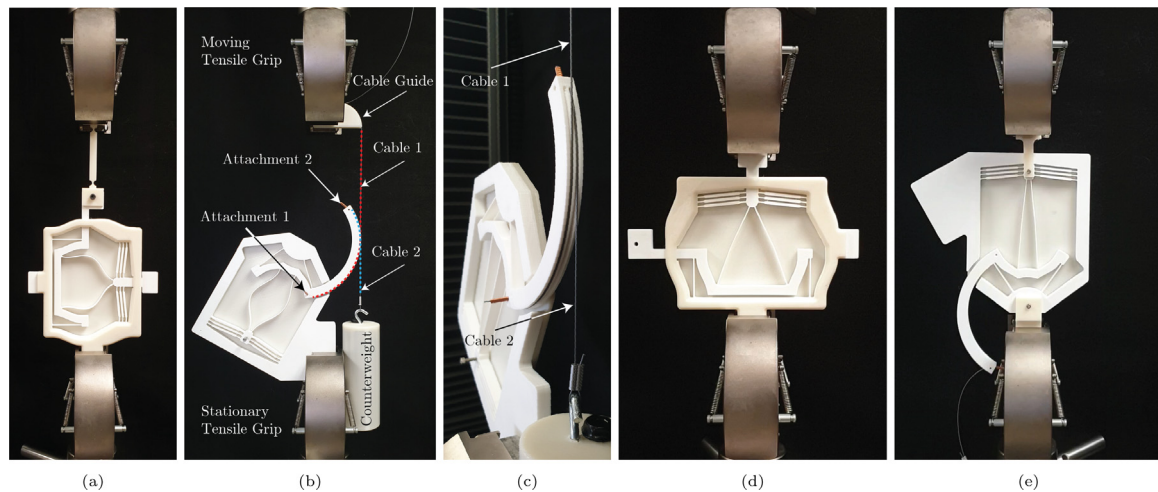

Fig. 3. (a) Shows the measurement setup of the linear device. (b) Shows the measurement setup for the rotary device with cable system and preloading weight. (c) Shows how the cables run along grooves in the circular arm of the rotary device. Bistability is measured for the linear device as shown in (d) and for the rotary device as shown in (e).

mechanisms (MSCMs) [12,49–51]. However, their direction of preloading is aligned with the intended mechanical mobility and can therefore not be controlled independently.

We propose to attach a MSCM to the negative stiffness device from Fig. 1(d). Since the direction of preloading and generated negative stiffness are perpendicular, preloading can be engaged and disengaged independently from the primary mobility. MSCMs are easily made fully compliant, because multistability is most often caused by snap-through of buckled beams [52]. This enables a monolithic system integration and hence miniaturization. Since only two stable states are required for binary stiffness, a bistable mechanism is used.

A myriad of bistable mechanisms are reported in literature both on large scale and small scale. Among them are chevron type bistable mechanisms [53,54], a curved beam bistable mechanism [55], a tensural bistable micro-mechanism [56], two-link in-plane bistable micro-mechanisms [57,58], bistable mechanisms based on slider mechanisms [59,60] and a rotational bistable mechanism [61].

Although the above bistable mechanisms are passive devices, active implementations are equally common. These microrelays can switch between stable states by means of actuation, but do not require actuation to stay in either state. A wide variety of actuator-mechanism combinations is reported in literature, including rotary bistable mechanisms [62]. Most microrelays rely for their bistability on a set of at least two curved or chevron style beams centrally connected to prevent rotation. Actuation is most commonly done by chevron type thermal actuators [63–67], but also with bending beam thermal actuators [68,69], external electromagnetic actuation [70,71,62], a combination of thermal and electromagnetic [72] and electrostatic comb actuators [73–76].

In our large scale design a passive chevron type bistable mechanism is implemented. Maximizing the force required to switch equilibrium is important, because a higher threshold force means more negative stiffness can be created. To do this multiple chevron bistable beams are used in parallel. Also, lumped compliance is used instead of distributed compliance to further increase the severity of the bistability by thickening the beams in the middle [53]. The exact dimensions are determined by iterative design in combination with a parametric finite element model.

2.2. Modeling, design and fabrication

Parametric finite element models of the proposed mechanisms are built in Ansys APDL out of two-node beam elements
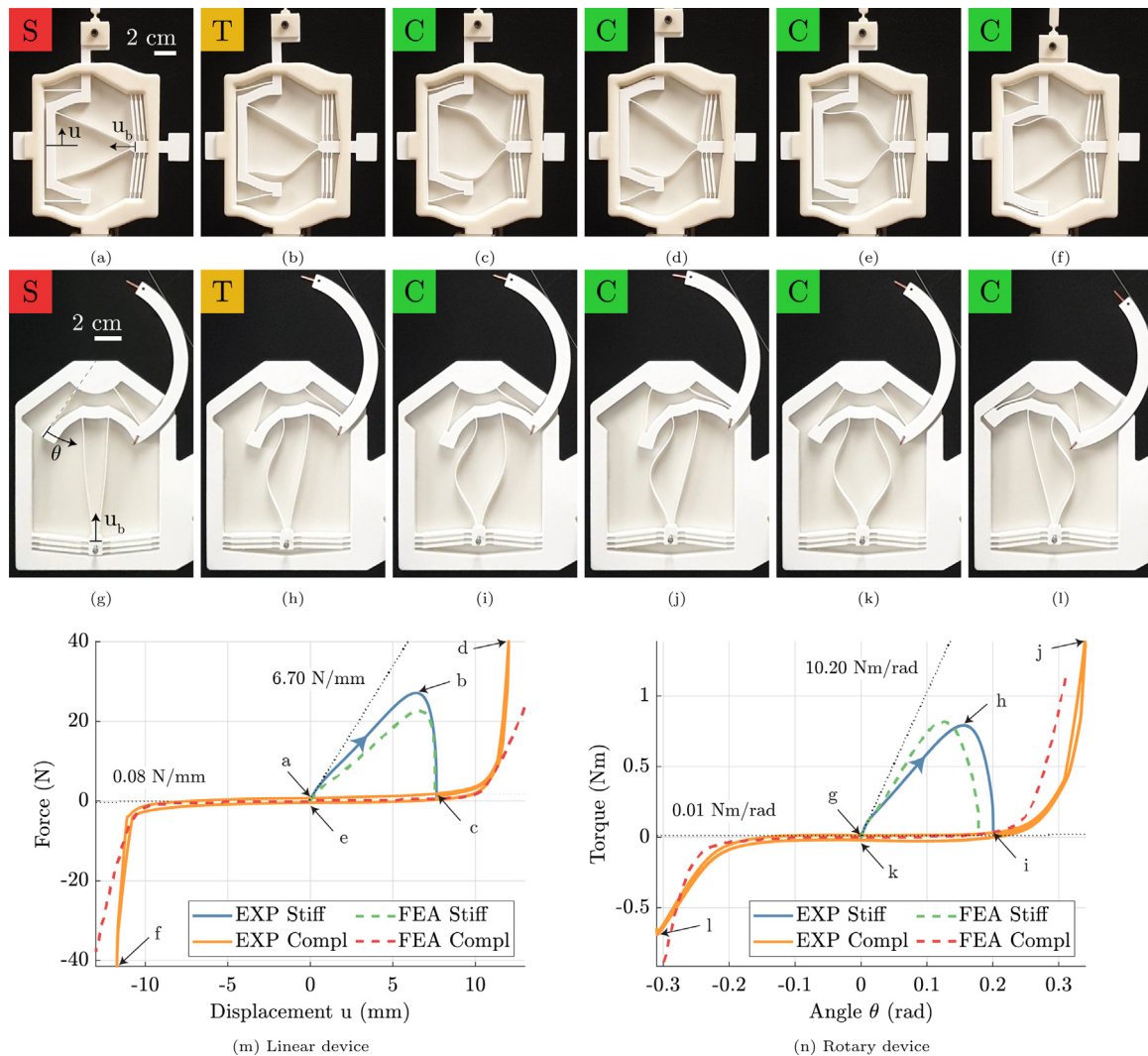
Fig. 4. A chronological photo sequence of the linear device (a–f) and the rotary device (g–l) taken during measurement. Three different states can be identified, a stable stiff configuration in red (S), an unstable transition state in which the bistable switch is toggling in yellow (T) and a stable compliant configuration in green (C). The different mechanism configurations are correspondingly indicated in the force deflection diagrams from (m) and (n) with both measurements (EXP) and finite element simulations (FEA). The stiffness in both stiff and compliant states around the equilibrium position are shown as dotted lines. (For interpretation of the references to color in this figure legend, the reader is referred to the web version of this article.)

(beam188) based on Timoshenko beam theory, a linear shape function and a rectangular cross section. The models are iteratively to create devices that approximate zero stiffness over a maximized range of motion. In practice this entails a design cycle in which a grid search is performed to determine dimensions, simulations ran and prototypes manufactured to validate simulations and build intuition for manufacturing and materials.

The model carefully takes into account the geometry of the flexible elements and models elastic boundary conditions. Supporting back and front plates are added to reinforce the frame, which is needed due to the gate allowing the main stage to exit the frame. The devices are grounded by constraining the motion of the lower left corner in all directions and the motion of the lower right corner in the vertical direction as shown in Figs. 2(a) and 2(f).

In order to compute post buckling behavior, imperfections are added to the bistable mechanisms [77]. A linear buckling analysis is first performed by adding a unit force on the bistable element. Next the first five normalized buckling mode shapes are added to the undeformed geometry with an amplitude of 0.01. Only then the bistable element is connected to the negative

stiffness structure. An element plot and a deformation plot in post buckling are shown in Figs. 2(a), 2(b), 2(f) and 2(g).

All plate springs have a beam thickness of 0.7 mm and are 7 mm high. The plate springs of the stages have a length of 35 mm and are at an angle of 70° for the rotational stage.

The angle α between the negative stiffness plate springs in the rectilinear case is 45° and they are 75 mm long. In case of rotation the plate springs are 89 mm long and the angle α between them is 10°. All negative stiffness plate springs have the shape of a cosine with an amplitude of 0.7 mm, making sure they will buckle outwards. Inwards buckling is prevented, because this may cause the V-shaped plate springs to touch each other and challenge performance by introducing for example friction and unwanted deformations. To save space, they are placed as far up as possible. The systems are designed for a range of motion of ±10 mm and ±0.2 rad (±11.5°) for translation and rotation. A fillet of at least 0.7 mm is added to each corner.

In both cases an identical bistable switch is used. Its parameters are chosen such that it can stay in either configuration without effort, while it maintains the load provided by the negative stiffness from the V-shaped plate spring. To create sufficient transition force within material limits, three parallel beams are
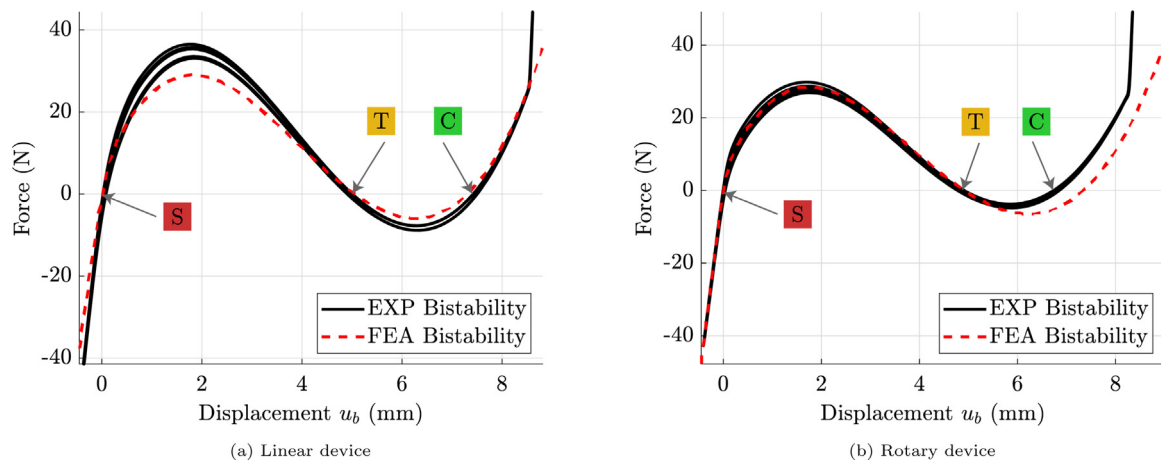
(a) Linear device

(b) Rotary device

Fig. 5. Measurement (EXP) and simulation (FEA) results of the bistable switch are in good agreement for both the linear (a) and rotary (b) device. All equilibrium points are associated with the different states, stiff (S), compliant (C) and toggle (T), as shown in Fig. 4.

used instead of two, similar to [53]. The flexures have a total length of 43 mm where the thick part is 31 mm long and 2 mm wide. The offset between the outside of the flexures and the shuttle in the middle is 4.5 mm, such that elastic equilibrium is found when preloaded between 7 mm and 8 mm, see Fig. 5.

The mechanisms are 3D printed by fused deposition modeling (FDM) on a Original Prusa i3 MK3S out of polylactic acid (PLA) with default settings. Isotropic material properties are assumed based on FDM printed PLA with a layer raster angle of 0° [78]. A Young's modulus of 3.12 GPa and an ultimate tensile stress of 50.23 MPa are used with a Poison's ratio of 0.3. A CAD drawing and photos of the fabricated linear and rotary devices are shown in Figs. 2(c)–2(e) and 2(h)–2(j).

2.3. Measurements

Force deflection measurements are done with an Instron 5966 tensile test bench. Transition from high to low stiffness is measured by actuating the linear stage bounded by a force of 40 N at a strain rate of 15 mm min^{-1}. Parasitic motion is accounted for by adding a follower beam between the clamp and the mechanism, see Fig. 3(a). Gravity is not accounted for.

By using a cable system, the rotational mechanism is measured on the same tensile test bench. Since cables cannot be loaded in compression, the combined system is preloaded in tension by a 10.2 N counterweight. Two cables run along grooves on an extended circular arm with a radius of 68.8 mm, see Figs. 3(b) and 3(c). Cable one (in red in Fig. 3(b)) runs from attachment one to the moving tensile grip that is attached to the force sensor. Cable two (in blue) runs from attachment two to the counterweight that preloads the cablesystem. A constant arm radius is assumed to compute the moments and angles from the measured forces and displacements.

Bistability is measured the same way, see Figs. 3(d) and 3(e).

3. Results

Measurement (EXP) and finite element simulation (FEA) results for the main stage, both linear and rotary, are shown in Fig. 4 and for the bistable switches in Fig. 5. All force displacement measurements are in good agreement with simulations.

The chronological photo sequences from Figs. 4(a)–4(f) and Figs. 4(g)–4(l) associate each mechanism state with a point on the force deflection graphs from Figs. 4(m) and 4(n). Three different mechanism configurations can be identified. The first (red S) is a stable configuration with high stiffness in which the device is

manufactured and thus stress free, see Figs. 4(a) and 4(g). The second (yellow T) is unstable in which the bistable switch is toggling, see Figs. 4(b) and 4(h). In this instantaneous state of transition the device is neither on nor off, but at the onset of snap through to either configurations. In the third configuration (green C) the bistable switch is toggled and the V-shaped plate spring buckled, it is highly compliant and also stable as shown in Figs. 4(c)–4(f) and 4(i)–4(l). The configurations are also indicated in the force deflection characteristics of the bistable switch from Figs. 5(a) and 5(b).

A dramatic reduction in stiffness can be readily observed. Around the equilibrium position at $(0, 0)$, translational stiffness is reduced by 98.8 % from 6.70 N mm^{-1} to 0.08 N mm^{-1} and rotational stiffness is reduced by 99.9 % from 10.20 N m rad^{-1} to 0.01 N m rad^{-1}. These states of stiffness differ by two and three orders of magnitude with a factor of 84 and 1020 respectively.

By pulling on the main stage a force and torque of 27.11 N and 0.79 N m are required to transition. However, if the bistable switch is directly actuated a force of 36.56 N and 29.81 N are required. By design the mechanisms cannot transition back from compliant to stiff by actuating the main stage, because the V-shaped plate spring cannot overcome the threshold force of the bistable switch. However, it is possible by directly actuating the bistable switch with -8.87 N and -4.82 N for the linear and rotary device, as can be seen in Figs. 5(a) and 5(b)

In each case the low stiffness domain is in accordance with the intended range of motion. In the linear case, low stiffness stretches 20 mm and by taking into account a 150 mm frame width (without the clamp brackets) this results in a relative range of motion of 13.3 %. The range of motion in the stiff configuration is approximately 14 mm or 9.3 %. In the rotary case, the low stiffness domain stretches 0.4 rad (23°) and high stiffness approximately 0.32 rad (18°). Beyond these ranges stiffness ramps up quickly and a slight discrepancy between measurement and simulation is observed. These differences may be attributed to issues such as parasitic motion and contact between frame and stage. Contact is also clearly observed at the right side of the curves in Fig. 5.

The discrepancy observed between the measurements and simulations of the stiff parts of Fig. 4, but also that of the bistability in Fig. 5, may be attributed to frame geometry. The stiffness of the boundary conditions of a bistable mechanisms are extremely important. If boundaries are too compliant, the bistable behavior may even disappear. Since we have only coarsely approximated the frame geometry, it would be possible to have a discrepancy between the modeled and actual frame stiffness, but the simulations show good agreement with the experiments.

4. Conclusion

In this paper we have introduced two mechanisms with binary stiffness that are essential building blocks for mechanical digital machines. Extreme states of linear and angular stiffness are achieved by enabling and disabling static balancing by engaging and disengaging preloading. A new V-shaped negative stiffness plate spring is used successfully to maximize the ratio between the two states of stiffness by controlling its preloading with a bistable switch.

Linear stiffness is reduced by 98.8% from $6.70\,\text{N}\,\text{mm}^{-1}$ to $0.08\,\text{N}\,\text{mm}^{-1}$ over an absolute range of motion of 20 mm and a relative range of motion of 13.3%. Angular stiffness is reduced by 99.9% from $10.20\,\text{N}\,\text{m}\,\text{rad}^{-1}$ to $0.01\,\text{N}\,\text{m}\,\text{rad}^{-1}$ over a range of 0.4 rad or 23°. This is a difference in stiffness by two and three orders of magnitude with a factor 84 and 1020 respectively. This is a significant improvement over previously reported statically balanced mechanisms with stiffness reduction factors of 46, −21.2, −4.2 and 3.3 with corresponding reduction percentages 97.8%, −104.7%, −123% and 70% from [48,79,47,45].

A force of 27.11 N and a torque of 0.79 N m on the main stage is required to transition irreversibly from high to low stiffness. Reversible transition is possible by actuating the bistable switch with 36.56 N and −8.87 N in the linear device, and 29.81 N and −4.82 N in the angular device. All measurements are in good agreement with simulations.

The presented mechanisms could set the stage for innovative mechanical logical systems, adaptive and programmable metamaterials and other types of mechanical digital machines. To enable miniaturization and micro-fabrication required for such machines we have carefully considered scalability. All required components are integrated in a single piece device that can be fabricated with conventional surface-micro-machining or upcoming micro 3D printing technologies. Although the introduced devices are passive, scaling down presents opportunities for actuator implementation by replacing the passive bistable switch with an active micro-relay commonly reported in scientific literature about MEMS.

Declaration of competing interest

The authors declare that they have no known competing financial interests or personal relationships that could have appeared to influence the work reported in this paper.

Acknowledgments

References

[1] M.L.C. de Laat, H.H.P. Garza, J.L. Herder, M.K. Ghatkesar, A review on in situ stiffness adjustment methods in mems, J. Micromech. Microeng. 26 (6) (2016) 063001, http://dx.doi.org/10.1088/0960-1317/26/6/063001.

[2] C.B. Churchill, D.W. Shahan, S.P. Smith, A.C. Keefe, G.P. McKnight, Dynamically variable negative stiffness structures, Sci. Adv. 2 (2) (2016) e1500778, http://dx.doi.org/10.1126/sciadv.1500778.

[3] B. Vanderborght, A. Albu-Schäffer, A. Bicchi, E. Burdet, D.G. Caldwell, R. Carloni, M. Catalano, O. Eiberger, W. Friedl, G. Ganesh, et al., Variable impedance actuators: A review, Robot. Auton. Syst. 61 (12) (2013) 1601–1614, http://dx.doi.org/10.1016/j.robot.2013.06.009.

[4] D. Hyun, H.S. Yang, J. Park, Y. Shim, Variable stiffness mechanism for human-friendly robots, Mech. Mach. Theory 45 (6) (2010) 880–897, http://dx.doi.org/10.1016/j.mechmachtheory.2010.01.001.

[5] T. Morita, S. Sugano, Design and development of a new robot joint using a mechanical impedance adjuster, in: Proceedings of 1995 IEEE International Conference on Robotics and Automation, Vol. 3, IEEE, 1995, pp. 2469–2475, http://dx.doi.org/10.1109/ROBOT.1995.525630.

[6] K. Kim, H. Heo, J. Ju, A mechanism-based architected material: A hierarchical approach to design Poisson's ratio and stiffness, Mech. Mater. 125 (2018) 14–25, http://dx.doi.org/10.1016/j.mechmat.2018.07.001.

[7] R. Poon, J.B. Hopkins, Phase-changing metamaterial capable of variable stiffness and shape morphing, Adv. Energy Mater. (2019) 1900802, http://dx.doi.org/10.1002/adem.201900802.

[8] Y. Shan, M. Philen, A. Lotfi, S. Li, C.E. Bakis, C.D. Rahn, K. Wang, Variable stiffness structures utilizing fluidic flexible matrix composites, J. Intell. Mater. Syst. Struct. 20 (4) (2009) 443–456, http://dx.doi.org/10.1177/1045389X08095270.

[9] Y. Song, P.C. Dohm, B. Haghpanah, A. Vaziri, J.B. Hopkins, An active microarchitectured material that utilizes piezo actuators to achieve programmable properties, Adv. Energy Mater. 18 (7) (2016) 1113–1117, http://dx.doi.org/10.1002/adem.201500607.

[10] L.A. Shaw, J.B. Hopkins, An actively controlled shape-morphing compliant microarchitectured material, J. Mech. Robot. 8 (2) (2016) http://dx.doi.org/10.1115/1.4031168.

[11] C. Luo, Y. Song, C. Zhao, S. Thirumalai, I. Ladner, M.A. Cullinan, J.B. Hopkins, Design and fabrication of a three-dimensional meso-sized robotic metamaterial with actively controlled properties, Mater. Horiz. 7 (1) (2020) 229–235, http://dx.doi.org/10.1039/C9MH01368G.

[12] P.J. Pluimers, N. Tolou, B.D. Jensen, L.L. Howell, J.L. Herder, A compliant on/off connection mechanism for preloading statically balanced compliant mechanisms, in: ASME 2012 International Design Engineering Technical Conferences and Computers and Information in Engineering Conference, American Society of Mechanical Engineers, 2012, pp. 373–377, http://dx.doi.org/10.1115/DETC2012-71509.

[13] K. Hoetmer, J.L. Herder, C.J. Kim, A building block approach for the design of statically balanced compliant mechanisms, in: ASME 2009 International Design Engineering Technical Conferences and Computers and Information in Engineering Conference, American Society of Mechanical Engineers, 2009, pp. 313–323, http://dx.doi.org/10.1115/DETC2009-87451.

[14] S. Groothuis, R. Carloni, S. Stramigioli, A novel variable stiffness mechanism capable of an infinite stiffness range and unlimited decoupled output motion, in: Actuators, Vol. 3, Multidisciplinary Digital Publishing Institute, 2014, pp. 107–123, http://dx.doi.org/10.3390/act3020107.

[15] J. van Eijk, J.F. Dijksman, Plate spring mechanism with constant negative stiffness, Mech. Mach. Theory 14 (1) (1979) 1–9, http://dx.doi.org/10.1016/0094-114X(79)90036-3.

[16] H. Zhao, D. Han, L. Zhang, S. Bi, Design of a stiffness-adjustable compliant linear-motion mechanism, Precis. Eng. 48 (2017) 305–314, http://dx.doi.org/10.1016/j.precisioneng.2016.12.013.

[17] R.H. Nathan, A constant force generation mechanism, Trans. ASME, J. Mech. Transm. Autom. Des. 107 (4) (1985) 508–512, http://dx.doi.org/10.1115/1.3260755.

[18] J.L. Herder, Energy-Free Systems. Theory, Conception and Design of Statically, Vol. 2, 2001.

[19] Y. Liu, D.-J. Li, D.-p Yu, J.-g Miao, J. Yao, Design of a curved surface constant force mechanism, Mech. Based Des. Struct. Mach. 45 (2) (2017) 160–172, http://dx.doi.org/10.1080/15397734.2016.1157692.

[20] S.T. Park, T.T. Luu, Techniques for optimizing parameters of negative stiffness, Proc. Inst. Mech. Eng. C 221 (5) (2007) 505–510, http://dx.doi.org/10.1243/0954406JMES390.

[21] P. Wang, Q. Xu, Design and modeling of constant-force mechanisms: A survey, Mech. Mach. Theory 119 (2018) 1–21, http://dx.doi.org/10.1016/j.mechmachtheory.2017.08.017.

[22] M. Schenk, S.D. Guest, On zero stiffness, Proc. Inst. Mech. Eng. C (2013) 0954406213511903, http://dx.doi.org/10.1177/0954406213511903.

[23] G. Chen, Q.T. Aten, S. Zirbel, B.D. Jensen, L.L. Howell, A tristable mechanism configuration employing orthogonal compliant mechanisms, J. Mech. Robot. 2 (1) (2010) http://dx.doi.org/10.1115/1.4000529.

[24] G. Chen, Y. Gou, A. Zhang, Synthesis of compliant multistable mechanisms through use of a single bistable mechanism, J. Mech. Des. 133 (8) (2011) http://dx.doi.org/10.1115/1.4004543.

[25] D. Younesian, M.-R Alam, Multi-stable mechanisms for high-efficiency and broadband ocean wave energy harvesting, Appl. Energy 197 (2017) 292–302, http://dx.doi.org/10.1016/j.apenergy.2017.04.019.

[26] M. Zanaty, S. Henein, Programmable constant-force multistable mechanisms, in: International Design Engineering Technical Conferences and Computers and Information in Engineering Conference, Vol. 51807, American Society of Mechanical Engineers, 2018, http://dx.doi.org/10.1115/DETC2018-85248, V05AT07A002.

[27] A. Ion, L. Wall, R. Kovacs, P. Baudisch, Digital mechanical metamaterials, in: Proceedings of the 2017 CHI Conference on Human Factors in Computing Systems, ACM, 2017, pp. 977–988, http://dx.doi.org/10.1145/3025453.3025624.

[28] R.C. Merkle, Two types of mechanical reversible logic, Nanotechnology 4 (2) (1993) 114, http://dx.doi.org/10.1088/0957-4484/4/2/007.

[29] J.S. Hall, Nanocomputers and reversible logic, Nanotechnology 5 (3) (1994) 157, http://dx.doi.org/10.1088/0957-4484/5/3/002.

[30] P.L. Bergstrom, T. Tamagawa, D.L. Polla, Design and fabrication of microme-chanical logic elements, in: IEEE Proceedings on Micro Electro Mechanical Systems, an Investigation of Micro Structures, Sensors, Actuators, Machines and Robots, IEEE, 1990, pp. 15–20, http://dx.doi.org/10.1109/MEMSYS.1990. 110239.

[31] Y. Song, R.M. Panas, S. Chizari, L.A. Shaw, J.A. Jackson, J.B. Hopkins, A.J. Pascall, Additively manufacturable micro-mechanical logic gates, Nature Commun. 10 (1) (2019) 882, http://dx.doi.org/10.1038/s41467-019-08678-0.

[32] A. Sharma, W.S. Ram, C. Amarnath, Mechanical logic devices and circuits, in: 14th National Conference on Machines and Mechanisms, NaCoMM-09, Durgapur, India, Dec, 2009, pp. 17–18.

[33] A. Modi, P.S. Gandhi, H. Shah, S.G. Singh, Design, analysis and fabrica-tion of microflexural not gate, in: ASME 2007 International Mechanical Engineering Congress and Exposition, American Society of Mechanical Engineers Digital Collection, 2007, pp. 501–508, http://dx.doi.org/10.1115/ IMECE2007-41713.

[34] A. Modi, H. Shah, C. Amarnath, P. Gandhi, S. Singh, R. Rashmi, Design, analysis and fabrication of a microflexural and gate, in: 13th National Conference on Mechanisms and Machines, NaCoMM-07, Bangalore, India, Dec, 2007, pp. 12–13.

[35] T.J. Thorp, G.S. Yee, C.M. Sechen, Design and synthesis of dynamic circuits, IEEE Trans. Very Large Scale Integr. (VLSI) Syst. 11 (1) (2003) 141–149, http://dx.doi.org/10.1109/TVLSI.2002.800518.

[36] K.E. Drexler, Rod logic and thermal noise in the mechanical nanocomputer, in: Proc. Third Int. Symp. on Molecular Electronic Devices, 1988.

[37] M.A.A. Hafiz, L. Kosuru, M.I. Younis, Microelectromechanical repro-grammable logic device, Nature Commun. 7 (1) (2016) 1–9, http://dx.doi. org/10.1038/ncomms11137.

[38] S. Chizari, L.A. Shaw, J.B. Hopkins, Simultaneous printing and deforma-tion of microsystems via two-photon lithography and holographic optical tweezers, Mater. Horiz. 6 (2) (2019) 350–355, http://dx.doi.org/10.1039/ c8mh01100a.

[39] M. Bessa, R. Bostanabad, Z. Liu, A. Hu, D.W. Apley, C. Brinson, W. Chen, W.K. Liu, A framework for data-driven analysis of materials under uncertainty: Countering the curse of dimensionality, Comput. Methods Appl. Mech. Engrg. 320 (2017) 633–667, http://dx.doi.org/10.1016/j.cma.2017.03.037.

[40] M.A. Bessa, P. Glowacki, M. Houlder, Bayesian machine learning in meta-material design: Fragile becomes supercompressible, Adv. Mater. 31 (48) (2019) 1904845, http://dx.doi.org/10.1002/adma.201904845.

[41] M.A. Bessa, S. Pellegrino, Design of ultra-thin shell structures in the stochastic post-buckling range using Bayesian machine learning and op-timization, Int. J. Solids Struct. 139 (2018) 174–188, http://dx.doi.org/10. 1016/j.ijsolstr.2018.01.035.

[42] J.A. Gallego, J.L. Herder, Criteria for the static balancing of compliant mechanisms, in: ASME 2010 International Design Engineering Technical Conferences and Computers and Information in Engineering Conference, American Society of Mechanical Engineers, 2010, pp. 465–473, http://dx. doi.org/10.1115/DETC2010-28469.

[43] J. Zhang, A.D. Shaw, M. Amoozgar, M.I. Friswell, B.K. Woods, Bidirectional torsional negative stiffness mechanism for energy balancing systems, Mech. Mach. Theory 131 (2019) 261–277, http://dx.doi.org/10.1016/j. mechmachtheory.2018.10.003.

[44] J.F. Dijksman, A Study of Some Aspects of the Mechanical Behaviour of Cross-Spring Pivots and Plate Spring Mechanisms with Negative Stiffness, 1979.

[45] F.M. Morsch, J.L. Herder, Design of a generic zero stiffness compliant joint, in: ASME 2010 International Design Engineering Technical Conferences and Computers and Information in Engineering Conference, American Society of Mechanical Engineers, 2010, pp. 427–435, http://dx.doi.org/10.1115/ DETC2010-28351.

[46] L. Berntsen, D.H. Gosenshuis, J.L. Herder, Design of a compliant mono-lithic internally statically balanced four-bar mechanism, in: ASME 2014 International Design Engineering Technical Conferences and Comput-ers and Information in Engineering Conference, American Society of Mechanical Engineers, 2014, http://dx.doi.org/10.1115/DETC2014-35054, V05AT08A040.

[47] M. Barel, D.F. Machekposhti, J. Herder, N. Tolou, M. Sitti, Perma-nent preloading by acceleration for statically balancing MEMS devices, in: 2018 International Conference on Reconfigurable Mechanisms and Robots, ReMAR, IEEE, 2018, pp. 1–11, http://dx.doi.org/10.1109/REMAR. 2018.8449866.

[48] P.R. Kuppens, J.L. Herder, N. Tolou, Permanent stiffness reduction by thermal oxidation of silicon, J. Microelectromech. Syst. 28 (5) (2019) 900–909, http://dx.doi.org/10.1109/JMEMS.2019.2935379.

[49] P.J. Pluimers, Design for Specified Stiffness in Precision Engineering, 2012.

[50] G. Chen, S. Zhang, Fully-compliant statically-balanced mechanisms without prestressing assembly: Concepts and case studies, Mech. Sci. 2 (2) (2011) 169–174, http://dx.doi.org/10.5194/ms-2-169-2011.

[51] N. Tolou, P. Estevez, J.L. Herder, Collinear-type statically balanced com-pliant micro mechanism (SB-CMM): Experimental comparison between pre-curved and straight beams, in: ASME 2011 International Design Engineering Technical Conferences and Computers and Information in Engineering Conference, American Society of Mechanical Engineers, 2011, pp. 113–117, http://dx.doi.org/10.1115/DETC2011-47678.

[52] G. Chen, Y. Gou, L. Yang, Research on multistable compliant mechanisms: The state of the art, in: Proceedings of the 9th International Conference on Frontiers of Design and Manufacturing, 2010, pp. 1–5.

[53] S.A. Zirbel, K.A. Tolman, B.P. Trease, L.L. Howell, Bistable mechanisms for space applications, PLoS One 11 (12) (2016) e0168218, http://dx.doi.org/ 10.1371/journal.pone.0168218.

[54] B.D. Jensen, M.B. Parkinson, K. Kurabayashi, L.L. Howell, M.S. Baker, Design optimization of a fully-compliant bistable micro-mechanism, in: Proceedings of ASME IMECE, vol. 2, 2001, pp. 2931–2937.

[55] J. Qiu, J.H. Lang, A.H. Slocum, A curved-beam bistable mechanism, J. Microelectromech. Syst. 13 (2) (2004) 137–146, http://dx.doi.org/10.1109/ JMEMS.2004.825308.

[56] D.L. Wilcox, L.L. Howell, Fully compliant tensural bistable micromecha-nisms (FTBM), J. Microelectromech. Syst. 14 (6) (2005) 1223–1235, http: //dx.doi.org/10.1109/JMEMS.2005.859089.

[57] B.D. Jensen, L.L. Howell, L.G. Salmon, Introduction of two-link in-plane, bistable compliant mems, in: Proceeding of the 1998 ASME Design Engineering Technical Conferences, DETC98/MECH-5837, 1998.

[58] B.D. Jensen, L.L. Howell, L.G. Salmon, Design of two-link, in-plane, bistable compliant micro-mechanisms, J. Mech. Des. 121 (3) (1999) 416–423, http: //dx.doi.org/10.1115/1.2829477.

[59] B.D. Jensen, Identification of Macro-And Micro-Compliant Mecha-nism Configurations Resulting in Bistable Behavior, Brigham Young University-Provo, 2003.

[60] B.D. Jensen, L.L. Howell, Bistable configurations of compliant mechanisms modeled using four links and translational joints, J. Mech. Des. 126 (4) (2004) 657–666, http://dx.doi.org/10.1115/1.1760776.

[61] R. Luharuka, P.J. Hesketh, Design of fully compliant, in-plane rotary, bistable micromechanisms for MEMS applications, Sensors Actuators A 134 (1) (2007) 231–238, http://dx.doi.org/10.1016/j.sna.2006.04.030.

[62] R. Luharuka, P.J. Hesketh, A bistable electromagnetically actuated rotary gate microvalve, J. Micromech. Microeng. 18 (3) (2008) 035015, http: //dx.doi.org/10.1088/0960-1317/18/3/035015.

[63] H. Huang, Y.-J. Yang, A mems bistable device with push-on–push-off capability, J. Microelectromech. Syst. 22 (1) (2012) 7–9, http://dx.doi.org/ 10.1109/JMEMS.2012.2228165.

[64] B.-T. Liao, H.-H. Shen, H.-H. Liao, Y.-J Yang, A bi-stable 2×2 optical switch monolithically integrated with variable optical attenuators, Opt. Express 17 (22) (2009) 19919–19925, http://dx.doi.org/10.1364/OE.17.019919.

[65] T. Gomm, L.L. Howell, R.H. Selfridge, In-plane linear displacement bistable microrelay, J. Micromech. Microeng. 12 (2002) 257, http://dx.doi.org/10. 1088/0960-1317/12/3/310.

[66] C. Lee, C.-Y Wu, Study of electrothermal V-beam actuators and latched mechanism for optical switch, J. Micromech. Microeng. 15 (1) (2004) 11, http://dx.doi.org/10.1088/0960-1317/15/1/003.

[67] M.S. Baker, L.L. Howell, On-chip actuation of an in-plane compliant bistable micromechanism, J. Microelectromech. Syst. 11 (5) (2002) 566–573, http: //dx.doi.org/10.1109/JMEMS.2002.803284.

[68] J. Qiu, J.H. Lang, A.H. Slocum, A.C. Weber, A bulk-micromachined bistable relay with u-shaped thermal actuators, J. Microelectromech. Syst. 14 (5) (2005) 1099–1109, http://dx.doi.org/10.1109/JMEMS.2005.856676.

[69] J. Qui, J.H. Lang, A.H. Slocum, R. Strumpler, A high-current electrothermal bistable MEMS relay, in: The Sixteenth Annual International Conference on Micro Electro Mechanical Systems, 2003. MEMS-03 Kyoto. IEEE, IEEE, 2003, pp. 64–67, http://dx.doi.org/10.1109/MEMSYS.2003.1189688.

[70] J.S. Ko, M.G. Lee, J.S. Han, J.S. Go, B. Shin, D.-S. Lee, A laterally-driven bistable electromagnetic microrelay, ETRI J. 28 (3) (2006) 389–392, http: //dx.doi.org/10.4218/etrij.06.0205.0138.

[71] D.-A. Wang, H.-T. Pham, Y.-H Hsieh, Dynamical switching of an electro-magnetically driven compliant bistable mechanism, Sensors Actuators A 149 (1) (2009) 143–151, http://dx.doi.org/10.1016/j.sna.2008.11.006.

[72] A. Cao, J. Kim, L. Lin, Bi-directional electrothermal electromagnetic actua-tors, J. Micromech. Microeng. 17 (5) (2007) 975, http://dx.doi.org/10.1088/ 0960-1317/17/5/018.

[73] R.A. Receveur, C.R. Marxer, R. Woering, V.C. Larik, N.-F. de Rooij, Laterally moving bistable MEMS DC switch for biomedical applications, J. Microelec-tromech. Syst. 14 (5) (2005) 1089–1098, http://dx.doi.org/10.1109/JMEMS. 2005.851843.

[74] M. Freudenreich, U. Mescheder, G. Somogyi, Simulation and realization of a novel micromechanical bi-stable switch, Sensors Actuators A 114 (2–3) (2004) 451–459, http://dx.doi.org/10.1016/j.sna.2004.01.034.

[75] J. Casals-Terre, A. Fargas-Marques, A.M. Shkel, Snap-action bistable micromechanisms actuated by nonlinear resonance, J. Microelectromech. Syst. 17 (5) (2008) 1082–1093, http://dx.doi.org/10.1109/JMEMS.2008.2003054.

[76] H.N. Kwon, I.-H. Hwang, J.-H. Lee, A pulse-operating electrostatic microactuator for bi-stable latching, J. Micromech. Microeng. 15 (8) (2005) 1511, http://dx.doi.org/10.1088/0960-1317/15/8/019.

[77] A. Dunning, N. Tolou, P. Pluimers, L. Kluit, J. Herder, Bistable compliant mechanisms: Corrected finite element modeling for stiffness tuning and preloading incorporation, J. Mech. Des. 134 (8) (2012) http://dx.doi.org/10.1115/1.4006961.

[78] C. Casavola, A. Cazzato, V. Moramarco, C. Pappalettere, Orthotropic mechanical properties of fused deposition modelling parts described by classical laminate theory, Mater. Des. 90 (2016) 453–458, http://dx.doi.org/10.1016/j.matdes.2015.11.009.

[79] A. Lamers, J.A.G. Sánchez, J.L. Herder, Design of a statically balanced fully compliant grasper, Mech. Mach. Theory 92 (2015) 230–239, http://dx.doi.org/10.1016/j.mechmachtheory.2015.05.014.